THE JOURNAL OF PHYSICAL CHEMISTRY C
A JOURNAL OF THE AMERICAN CHEMICAL SOCIETY

pubs.acs.org/JPCC

Article

Orientation of Few-Layer MoS_2 Films: In-Situ X-ray Scattering Study During Sulfurization

Ashin Shaji, Karol Vegso, Michaela Sojkova, Martin Hulman, Peter Nadazdy, Peter Hutar, Lenka Pribusova Slusna, Jana Hrda, Michal Bodik, Martin Hodas, Sigrid Bernstorff, Matej Jergel, Eva Majkova, Frank Schreiber, and Peter Siffalovic*

Cite This: J. Phys. Chem. C 2021, 125, 9461−9468

Read Online

ACCESS | Metrics & More | Article Recommendations | Supporting Information

ABSTRACT: Some of the distinct optical, catalytical, and electronic properties of few-layer MoS_2 films arise from a specific orientation of the MoS_2 layers. The growth of horizontally or vertically aligned MoS_2 during the sulfurization of predeposited Mo film can be controlled by various physical conditions such as temperature, heating rate, Mo film thickness, or sulfur vapor pressure. However, due to the inherent limitations of performing real-time and *in situ* experiments during sulfurization in a standard growth chamber, only a limited number of analytical techniques can be used to elucidate the in-process phase transformation. Here, we present a comprehensive real-time study of the growth of few-layer MoS_2 films by sulfurization of Mo films using *in situ* grazing-incidence wide-angle X-ray scattering. We demonstrate that the process gas flow, and thus the sulfur partial vapor pressure, is the key control parameter for the few-layer MoS_2 layer orientation while all other process parameters remain fixed. Tracking the crystallization of few-layer MoS_2 layers in real-time allowed us to estimate the activation energy required for both horizontal and vertical orientations. Growth of either horizontal or vertical MoS_2 was observed without a metastable transition between them throughout the sulfurization.

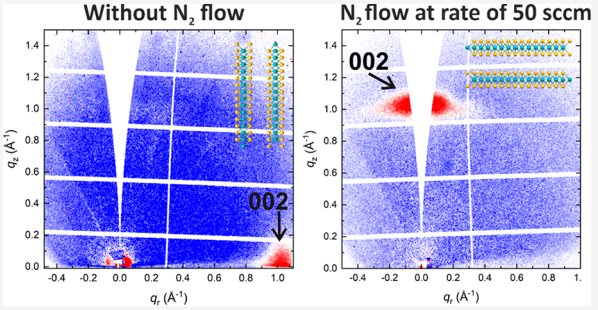

INTRODUCTION

MoS_2, a promising member of the transition metal dichalcogenide (TMD) family, draws serious attention of the scientific community due to its unique optical, electrical, and catalytic properties. The presence of van der Waals (vdW) forces between the weakly bound two-dimensional (2D) molecular layers in the TMDs makes them unique compared to their bulk counterparts.[1,2] TMD materials consist of a layered structure and have the general formula MX_2, where M represents a transition metal (Mo or W) and X refers to a chalcogen (S, Se, or Te). In MoS_2, the presence of a strong ionic bonding between the Mo and S atoms along with the presence of a weak vdW force between the different layers of MoS_2 enables thickness-dependent thermal, band gap and optical properties.[3−5] Numerous methods are available to produce few-layer or monolayer MoS_2 such as pulsed laser deposition,[6] exfoliation of bulk crystals,[4,7] or chemical vapor deposition (CVD).[8,9] CVD is an established technique for the fabrication of MoS_2 films with control over grain size,[10] layer numbers,[11] nucleation,[12] and lattice-orientation[13] by means of the growth parameters. Choudhary et al.[14] confirmed the influence of strain energy build-up during the growth on 2D layer orientation and the growth mode. It is already well reported that TMD materials with a hexagonal close-packed structure like MoS_2 layers can grow with horizontal or vertical alignment depending on the fabrication conditions. In the horizontal alignment (HA), the basal planes of the MoS_2 layers are oriented parallel to the substrate surface and the crystallographic *c*-axis is aligned along the substrate surface normal. HA MoS_2 layers are widely used in the field of optoelectronics[3,4] and electronics.[15,16] In the vertical alignment (VA), however, the basal planes are perpendicular to the substrate surface and the *c*-axis is perpendicular to the surface normal. VA MoS_2 layers are gaining particular interest due to their chemically reactive edges, which can be used for solar cells,[17] water disinfection,[18] water splitting,[19] and hydrogen evolution reactions (HER).[20] The spatial orientation of MoS_2 layers is important in determining the applications of this material.[21,22] Therefore, precise control over the growth orientations of these 2D TMD materials is critical to optimize their desired material properties and device functionalities.

Due to the scientific and technological importance of this promising material, numerous studies have already been

Received: February 25, 2021
Revised: April 15, 2021
Published: April 27, 2021

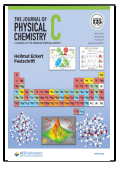

https://doi.org/10.1021/acs.jpcc.1c01716
J. Phys. Chem. C 2021, 125, 9461−9468

performed to investigate the underlying growth control parameters and their influence on the growth mechanisms. Two-zone sulfurization,[23] which is already a standard method for growing MoS_2 layers, is effective and reliable for the fabrication of HA and VA MoS_2 layers. A large class of parameters responsible for the observed growth of HA and VA-MoS_2 layers has not yet been fully explored.[18,20,24] On the basis of the previous studies, it turns out that the main process controlling the formation of either HA or VA growth is the diffusion of S into Mo, depending on the temperature and local concentration of S.[20,25] The thickness of the initial Mo layer is also a crucial parameter for determining the growth mode.[24] For thicker ($\gtrsim$ 3 nm) Mo layers, VA growth is dominant, whereas HA growth occurs for thinner layers. Other key factors controlling the growth of MoS_2 include pressure, temperature, and local sulfur concentration gradient in the sulfurized film and substrate.[26] In addition to this, Shang et al.[26] proposed Mo diffusion as a controlling factor for MoS_2 growth due to the extremely low diffusivity of Mo compared to sulfur.

It is widely accepted that the formation of VA MoS_2 in a two-zone furnace is mainly driven by rapid sulfur diffusion along vdW gap.[18,20,24] In that case, the annealing temperature is selected in the range from 500 to 800 °C and a short annealing time (10−20 min) is applied. VA MoS_2 was observed for a fast heating rate (in the order of tens of Kelvin per minute)[27] and when the thickness of Mo films exceeds 3 nm. Sojkova et al.[9] reported the transformation from VA to HA MoS_2 layer alignment by decreasing the heating rate while sulfurizing Mo films of the same thickness (3 nm). However, the role of sulfur partial vapor pressure (or sulfur concentration or carrier gas flow rate) on MoS_2 growth is by far less explored than the other growth parameters. Bo Chen et al.[28] demonstrated the preparation of large-area uniform monolayer MoS_2 films by an atmospheric pressure CVD method. They were able to control the sulfur partial vapor pressure by a sulfur vapor counterflow diffusion setup, which lowers the sulfur concentration in the reaction zone. Therefore, the sulfur partial vapor pressure seems to be another critical factor influencing the growth of MoS_2 films, but its effect on the growth orientation is relatively unexplored.

Here, we present a one-zone CVD method leading to the growth of either HA or VA MoS_2 films by sulfurizing Mo films with the same thickness. The sulfur powder was located directly under the Mo film substrate. The only control parameter is the sulfur vapor pressure, while the deposition temperature and heating rate were kept constant. Our investigations are supported by real-time and *in situ* grazing-incidence wide-angle X-ray scattering (GIWAXS). We observed the growth of either HA or VA MoS_2 as a function of sulfur partial vapor pressure controlled by the nitrogen flow through the CVD chamber. No metastable states or transitions between the two alignments were observed. To acquire a complete picture, we also calculated the activation energy for each case by mathematical modeling. Our observations confirm a sulfur diffusion-driven growth of HA and VA MoS_2 layers starting from the interface into the bulk of the Mo layers, while the final orientation is determined by a delicate balance between the film's surface energy and sulfurization rate given by the sulfur concentration at the vapor−solid interface. This breakthrough monitoring of phase transformations directly in a CVD chamber using the real-time GIWAXS technology described here is not limited to this particular system. In fact, it has more general consequences that can also be applied to other thin film growth processes.

EXPERIMENTAL DETAILS

Preparation of MoS_2 Layers. The few-layer MoS_2 films were prepared on *c*-plane sapphire substrates by sulfurization of Mo layers with a thickness of 3 nm. The dimensions of the sapphire substrates were 1 × 1 cm^2. The Mo layers were deposited by DC magnetron sputtering, and details can be found in ref 9. The few-layer MoS_2 films were prepared by one-zone sulfurization in a specially designed CVD reactor (Figure 1). Sulfur powder (0.5 g) was heated next to the sample placed near the center of the CVD reactor.

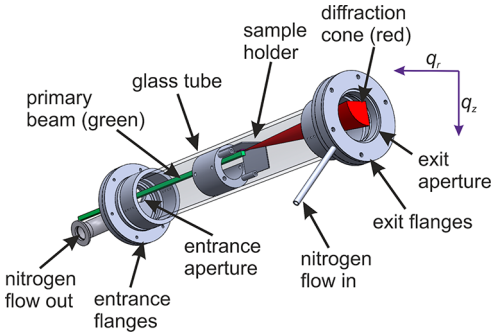

Figure 1. Schematic illustration of the core of a CVD reactor with sample holder, consisting of a glass tube enclosed by aluminum windows attached to the inlet and outlet flanges. Note that the sample was oriented downward with the normal of the sample along the q_z direction.

***In-situ* Synchrotron GIWAXS Measurements.** *In situ* GIWAXS measurements were performed at the SAXS beamline of the Elettra synchrotron radiation facility in Trieste, Italy. X-ray photons with an energy of 16 keV (wavelength of 0.7749 Å) were used. The photon flux on the sample was approximately 10^{12} photons/s. The X-ray beam size was adjusted to 3 mm × 1 mm (H × V) by a slit system. The X-ray beam divergence was 0.6 mrad × 0.3 mrad (H × V). The quartz tube of the CVD reactor shown in Figure 1 was inserted into the heating chamber as shown in Figure S1. The experimental details of the sample holder assembly are shown in Figure S2. The entire system was mounted on a heavy-duty hexapod (H-840, PI) with six-axis freedom, which allowed us to adjust the sample to the X-ray beam and set an angle of incidence of 0.2°. A transparent quartz glass tube was equipped on both sides with aluminum windows with a thickness of 30 μm, showing X-ray transparency of 95% for 16 keV photon energy. The windows were attached to the quartz tube by stainless steel flanges with O-ring Viton seals. The entrance and exit windows had a diameter of 20 mm and 55 mm, respectively. The sample was mounted on a stainless steel holder placed above the sulfur crucible, and the normal to the sample surface was oriented in the vertical direction (Figure 1). The inert atmosphere in the CVD tube was maintained by nitrogen at a flow rate of 50 sccm and a pressure of 0.5 bar for HA MoS_2 and no flow for VA MoS_2. The sample-to-detector distance was fixed to 845 mm. The X-ray detector used in the experiment was a CMOS-based Pilatus3 1 M (Dectris, Switzerland). The pixel size of the detector was 172 μm × 172 μm (H × V) with a total sensor area of 168.7 × 179.4 mm^2 (981 × 1043 pixels, H × V). The scattered X-ray intensity

https://doi.org/10.1021/acs.jpcc.1c01716
J. Phys. Chem. C 2021, 125, 9461−9468

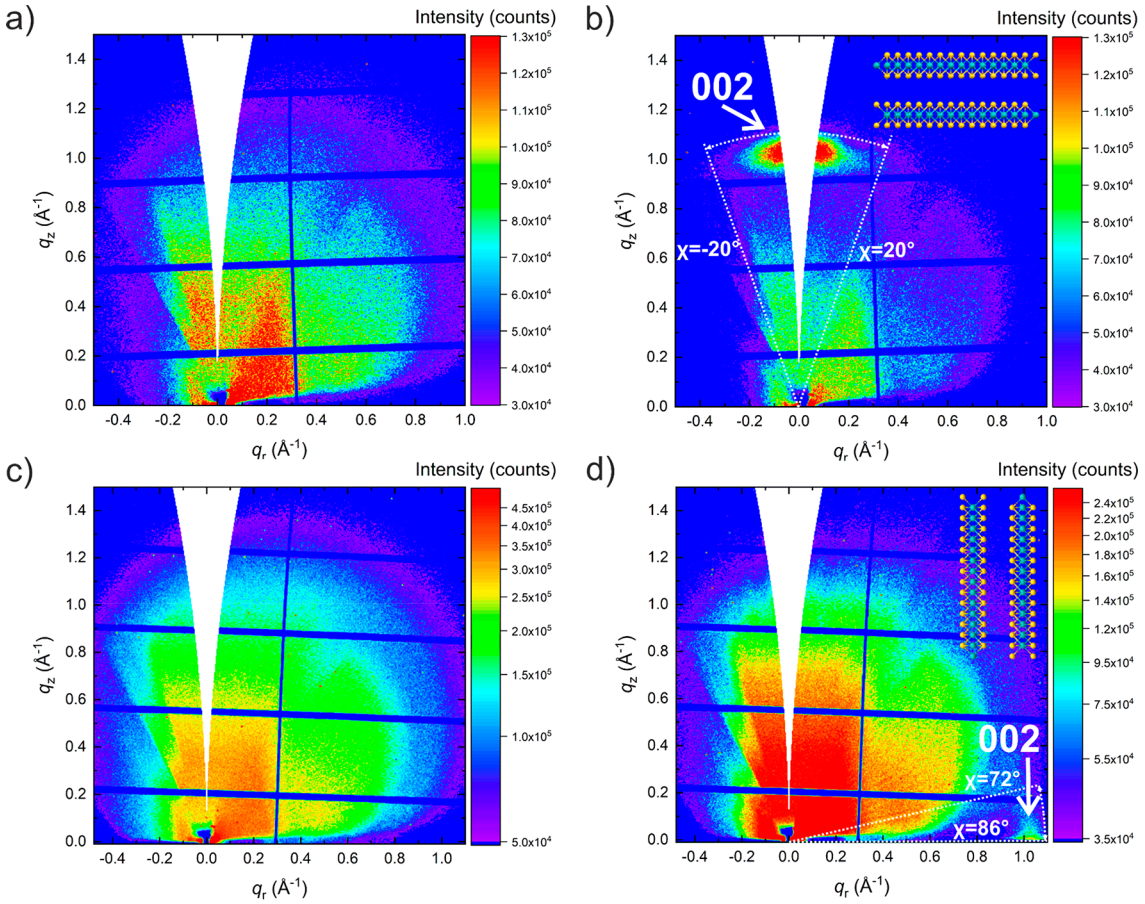

Figure 2. Sulfurization of Mo films at two different N_2 flows. GIWAXS patterns of (a) initial Mo and (b) final HA MoS_2 film after sulfurization at a flow rate of 50 sccm and (c) initial Mo and (d) final VA MoS_2 film after sulfurization at zero flow rate. The insets illustrate the orientation of MoS_2 layers. The dashed lines indicate the limits for profile integration.

was acquired continuously with an exposure time of 10 and 5 s for the growth of HA MoS_2 and VA MoS_2, respectively. During the in situ experiment, systematic sample displacement was observed due to thermal expansion of the mounting assembly, which was compensated by counter-movement of the entire CVD chamber using the hexapod.

RESULTS AND DISCUSSION

Our study was performed in a custom-designed CVD chamber dedicated to real-time and *in situ* GIWAXS. Figure 1 shows the schematic illustration of the experimental setup described in detail in Experimental Details and Supporting Information. The GIWAXS patterns are represented in reciprocal space, where the q_z and q_r coordinates denote the scattering along the substrate normal and in the substrate plane, respectively. The GIWAXS patterns taken before and after sulfurization of Mo films at a nitrogen flow rate of 50 sccm are shown in Figure 2a,b, respectively. The subtracted GIWAXS pattern between the final and initial states at this flow rate is shown in Figure S3a. After sulfurization, the layer shows a strong 002 diffraction spot located along the q_z direction at q_z = 1 Å^{-1}. This suggests that the (001) lattice planes of MoS_2 are oriented parallel to the sample surface with the *c*-axis oriented along the substrate surface normal, corresponding to HA MoS_2 films. On the other hand, GIWAXS patterns recorded before and after sulfurization of Mo films at zero nitrogen flow rate are shown in Figure 2c,d, respectively. The subtracted GIWAXS pattern between the final and initial states at zero flow rate is shown in Figure S3b. The 002 diffraction spot oriented along the q_r direction at q_r = 1 Å^{-1} confirms a perpendicular orientation of the (001) lattice planes with respect to the sample surface with the *c*-axis aligned in the plane of the film, which corresponds to VA MoS_2 films. We note that elastic X-ray scattering of the primary beam in nitrogen atmosphere of the CVD chamber is responsible for the strong observed intensity close to the origin of reciprocal space in all GIWAXS patterns. Furthermore, the inaccessible region of GIWAXS pattern along the q_z direction at q_r = 0 Å^{-1}, also known as the missing wedge, which is inherent to the scattering geometry used, prevents a direct comparison of the total phase volumes in HA and VA MoS_2 films.[29] However, this specific limitation of the GIWAXS measurement geometry does not prevent a comparison of the relative kinetics of the phase transformations during films sulfurization as described in the next section.

The CVD heating ramp of 25 °C/min and the maximum temperature of 600 °C held for 30 min were identical for both orientations of MoS_2. In the HA MoS_2 sample, the inert atmosphere inside the CVD chamber was maintained with a nitrogen flow rate of 50 sccm; this reduced the sulfur vapor partial pressure on the sample. On the other hand, for VA MoS_2 no nitrogen flow through the CVD reactor was used. Instead, it was only purged with nitrogen before the heating process. Possible gas backflow was prevented by using a one-way valve at the outlet of the CVD chamber. Consequently, the

https://doi.org/10.1021/acs.jpcc.1c01716
J. Phys. Chem. C 2021, 125, 9461−9468

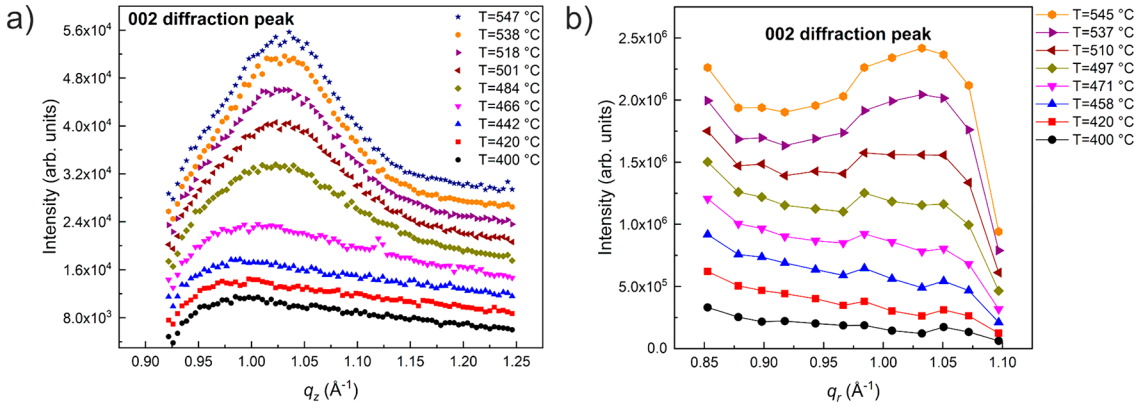

Figure 3. The 002 intensity profiles for (a) HA MoS_2 and (b) VA MoS_2 films at different temperatures.

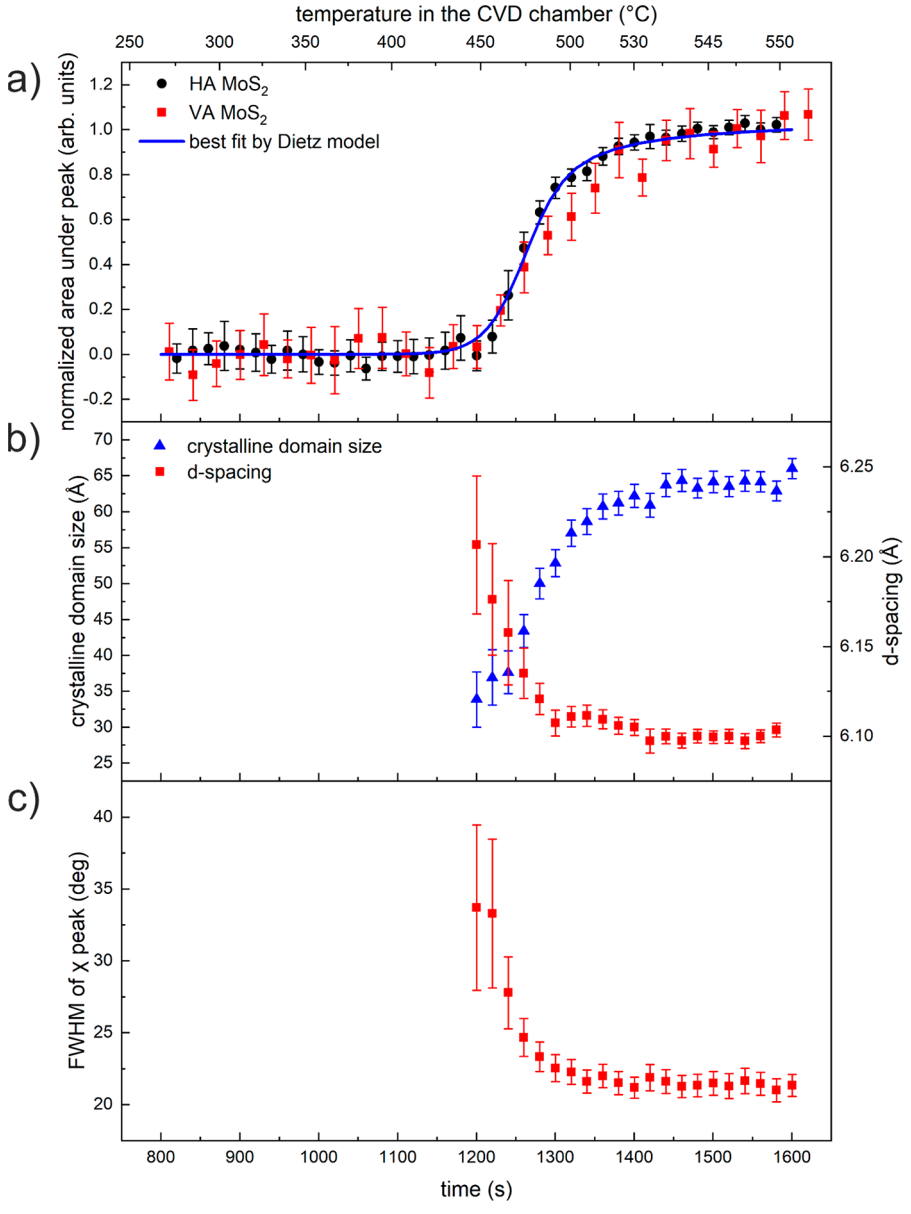

Figure 4. (a) The normalized 002 intensity for HA and VA MoS_2 layers as a function of time and temperature. The blue line renders the best fit by the Dietz model for the growth of HA MoS_2. (b) The calculated coherent crystalline domain size along with *d*-spacing and (c) fwhm of χ profiles as a function of time and temperature.

https://doi.org/10.1021/acs.jpcc.1c01716
J. Phys. Chem. C 2021, 125, 9461−9468

sulfur partial vapor pressure on the sample was higher throughout VA MoS_2 growth than during HA MoS_2 growth.

In order to quantify the temporal evolution of the Mo phase transformation during sulfurization, we extracted a series of reciprocal space cuts and evaluated them as a function of time. The selected intensity profiles of the 002 diffraction spot taken along the q_z direction in the χ range (−20°, +20°) during the phase transformation leading to HA MoS_2 are shown in Figure 3a. A detailed description of the χ-profiles extraction can be found in Supporting Information. For comparison, intensity profiles extracted along the q_r (i.e., in-plane) direction of the χ-range (72°, 86°) shown in Figure 3b were used to follow the Mo phase transformation toward VA MoS_2. In the case of VA MoS_2 films, the randomly oriented c-axis in the film plane and the grazing-incidence measurement geometry result in a much lower intensity of the 002 diffraction compared to that of the HA MoS_2 film. In both cases, the onset of the early phase transformation toward the MoS_2 phase can be already seen at close to 450 °C. The evaluation of the phase diagram of the Mo−S system[26,30] in the sulfur-rich region (S/Mo > 2) under a pressure of 1 atm reveals a universal CVD growth window for the MoS_2 phase from sulfur gas starting at 444.6 °C, which coincides well with the onset of the phase transition observed in our experiment. The phase transition reaches saturation for temperatures above 500 °C. The gradual narrowing of the 002 diffraction peak indicates an increasing size of coherently scattering domains of MoS_2 crystals in both films. A key observation in our experiments is the growth of either exclusively HA or exclusively VA MoS_2 phases. No reorientations between the two were detected during sulfurization. This suggests that the final orientation is determined by the extent of the sulfur diffusion from the vapor−solid interface into the bulk,[27,31] driven by the sulfur vapor pressure alone, since the solubility of sulfur in molybdenum is negligible.[32] Also, apparently once the growth of a given orientation has nucleated, there is no possibility of switching back. However, this observation, which applies to the formation of few-layer MoS_2, cannot be generally extended to the sulfurization of thick Mo films.

To provide a quantitative analysis of phase transformations for both orientations, the normalized integral intensities of the 002 diffraction peaks for HA and VA MoS_2 are plotted as functions of time and temperature in Figure 4a. Both HA and VA aligned MoS_2 samples show a similar evolution of the area under the 002 diffraction peak.

To facilitate the understanding of the phase transformations in both cases and to quantify the analysis, we implemented the mathematical models developed by Avrami and Dietz.[33−37] The activation energy was determined by applying the Avrami model since it provides the most straightforward crystallization kinetics model. As a first approximation, we used the Avrami model to fit the degree of phase conversion α as a function of time

$$\alpha(t) = 1 - e^{(-1)mIA\int X(t)\mathrm{d}t} \quad (1)$$

$$X(t) = e^{(-E/RT(t))}t^{m-1} \quad (2)$$

where m is the dimensionality of the growth (m = 3 in our case; see below), E is the activation energy, R is the universal gas constant, T is the temperature, A is the pre-exponential factor, and I is the integral area under the 002 diffraction peak.[38] The functional dependence $\alpha(t)$ was intentionally split into two parts to allow a simpler representation by an auxiliary function $X(t)$.

In the modeling, the temperature was considered to be linear with time. The Avrami model provided activation energies of 324 ± 2 and 329 ± 3 kJ mol^{-1} for HA and VA MoS_2, respectively. The published values of activation energies[31,32,39] for sulfurization of bulk Mo films range from 105 to 326 kJ mol^{-1}. On the basis of the measured values of activation energies for both orientations, it can be concluded that the growth of differently oriented MoS_2 has very similar activation energies within their corresponding confidence intervals. Since the only different growth parameter was the nitrogen gas flow, the origin of the different orientation should therefore be seen in the different sulfur vapor pressure. To further support our conclusions on the influence of the sulfur vapor pressure on the formation of differently oriented MoS_2 phases, we performed *in situ* X-ray absorption measurements of the process gas atmosphere directly in the CVD chamber (Supporting Information). The X-ray absorption measurements confirm an increased sulfur vapor pressure for VA MoS_2 growth compared to HA MoS_2 growth.

In the following, due to the better statistics of the scattered X-ray data for the growth of HA MoS_2 and similarities in the activation energies with VA MoS_2 we have performed the refined fitting procedure only for HA MoS_2 films. All diffraction peaks were fitted with a linear background. The Avrami model was successful in describing the initial stage of transformation kinetics. However, it fails to describe the slowdown of the crystallization process at the temperatures above the phase transition in the range between 500 and 550 °C, also known as the secondary or post-Avrami crystallization.[36−38] To overcome this drawback of the Avrami model, a modified Avrami model, so-called Dietz model, was applied.[4] The best fit of the Dietz model for HA MoS_2 is shown by the blue curve in Figure 4a, which was obtained for the parameter a = 0.9 (an explanation can be found in Supporting Information), dimensionality m = 3, and activation energy 321 ± 1.3 kJ mol^{-1}. However, as can be seen the application of the refined Dietz model does not change the activation energies and only influences the secondary crystallization rate as expected.

A rapid increase of the 002 diffraction intensity occurs between 450 and 500 °C. Moreover, in this temperature range, we observe almost a doubling of the average coherent crystalline domain size from about 30 Å to almost 60 Å, as shown in Figure 4b. This indicates the growth of MoS_2 nuclei from the vapor−solid interface of the Mo layer in this temperature range. Simultaneously, there is a decrease of the (002) interplanar spacing from an initial 6.2 ± 0.05 Å to a consolidated bulk value of 6.1 ± 0.01 Å. On the other hand, in the secondary crystallization stage above 500 °C, the further growth of the coherent crystalline domain size implies crystal coarsening with increasing temperature. At this stage, no significant change in the (002) interplanar spacing parameter can be detected. The simple Avrami model fails to describe exactly this phase, and the use of a more advanced Dietz model allows a good fit to the data even in this secondary crystallization phase without influencing the activation energies.

Finally, to assess the change in film mosaicity $\Delta\chi$ during the film sulfurization, that is, the mean misalignment of the crystal c-axis with respect to the surface normal, we extracted χ-cuts from the GIWAXS patterns as described in the Supporting

https://doi.org/10.1021/acs.jpcc.1c01716
J. Phys. Chem. C 2021, 125, 9461−9468

Information. For the growth of HA MoS_2, fwhm of the χ-cuts integrated in the q-range of 0.95−1.1 $Å^{-1}$ are shown in Figure 4c. We observe a decreasing angular misalignment $\Delta\chi$ of MoS_2 crystals from the substrate surface's normal direction in the primary phase of nucleation and crystal growth. The mean value of $\Delta\chi$ drops by more than 15° in the temperature range between 450 and 500 °C. In the following secondary crystallization stage, no significant changes in crystal orientations were observed.

Within the limits of our investigations, the observed difference in the growth of HA versus VA MoS_2 depends solely on the concentration of S atoms at the vapor−solid interface, since all other reaction parameters were kept constant. The growth of either HA or VA MoS_2 is controlled by a balance between the surface energy of the final film and the reactivity of Mo with S, which is limited by the diffusion of S atoms into the Mo bulk. The surface energy of VA films is less favorable compared to HA films because the edge sites surface energy is nearly 2 orders of magnitude above that of the basal plane.[40] This is also the reason why thin Mo films almost exclusively sulfurize in HA configuration.[24] On the other hand, in the limit of the thick films the enhanced diffusion of S atoms along the vdW gap favors the growth of VA MoS_2 films.[20,27] The evidence from this study suggests that the growth of VA MoS_2 at high S concentration is preferable to HA due to the efficient and rapid growth of MoS_2 phase. In this case, the fast diffusion kinetics of S into Mo bulk due to high sulfur pressure, forming MoS_2 phase, even prevailed over the lower surface energy offered by the alternative HA configuration. In contrast, under S deficient conditions induced by N_2 flow, the lower surface energy of the HA configuration outweighs the rapid diffusion-driven growth of the VA configuration.

CONCLUSIONS

Control over the orientation of few-layer MoS_2 films plays a crucial role in determining their applications. We performed a controlled sulfurization of Mo-coated substrates in a one-zone CVD furnace by fixing all parameters except the nitrogen flow through the reactor. We established that in the case of rapid sulfurization, the sulfur partial vapor pressure is the key parameter that determines the orientation of the final few-layer MoS_2 films. HA and VA MoS_2 films were fabricated with a nitrogen flow of 50 sccm and without flow, respectively. The activation energies of Mo sulfurization leading to HA or VA MoS_2 appear to be essentially identical, as evidenced by *in situ* GIWAXS. The origin of the different MoS_2 orientations at different sulfur vapor pressures can be explained by the competition between the fast sulfur diffusion along the vdW gap and surface energy minimization leading to VA or HA MoS_2, respectively. The presented real-time GIWAXS method opens the possibility to study the mechanisms behind the phase transformations in a large number of low-dimensional materials in CVD reactors in general. While the present results have important implications for a deeper understanding of the delicate balance between the growth of HA and VA MoS_2, further experimental and theoretical studies are required to fully understand the mechanisms underlying the findings.

ASSOCIATED CONTENT

Supporting Information

The Supporting Information is available free of charge at https://pubs.acs.org/doi/10.1021/acs.jpcc.1c01716.

Experimental details and additional explanation of data analysis and fitting (PDF)

AUTHOR INFORMATION

Corresponding Author

Peter Siffalovic − *Institute of Physics, Slovak Academy of Sciences, 84511 Bratislava, Slovakia; Centre for Advanced Materials Application, 84511 Bratislava, Slovakia;* orcid.org/0000-0002-9807-0810; Phone: +421-2-20910766; Email: peter.siffalovic@savba.sk; Fax: +421-2-54776085

Authors

Ashin Shaji − *Institute of Physics, Slovak Academy of Sciences, 84511 Bratislava, Slovakia*

Karol Vegso − *Institute of Physics, Slovak Academy of Sciences, 84511 Bratislava, Slovakia; Centre for Advanced Materials Application, 84511 Bratislava, Slovakia;* orcid.org/0000-0003-2595-6036

Michaela Sojkova − *Institute of Electrical Engineering, Slovak Academy of Sciences, 84104 Bratislava, Slovakia;* orcid.org/0000-0002-7490-3240

Martin Hulman − *Institute of Electrical Engineering, Slovak Academy of Sciences, 84104 Bratislava, Slovakia;* orcid.org/0000-0002-5598-9245

Peter Nadazdy − *Institute of Physics, Slovak Academy of Sciences, 84511 Bratislava, Slovakia; Institute of Electrical Engineering, Slovak Academy of Sciences, 84104 Bratislava, Slovakia*

Peter Hutar − *Institute of Electrical Engineering, Slovak Academy of Sciences, 84104 Bratislava, Slovakia*

Lenka Pribusova Slusna − *Institute of Electrical Engineering, Slovak Academy of Sciences, 84104 Bratislava, Slovakia;* orcid.org/0000-0002-4653-4492

Jana Hrda − *Institute of Electrical Engineering, Slovak Academy of Sciences, 84104 Bratislava, Slovakia*

Michal Bodik − *Institute of Physics, Slovak Academy of Sciences, 84511 Bratislava, Slovakia; Centre for Advanced Materials Application, 84511 Bratislava, Slovakia;* orcid.org/0000-0002-6518-7617

Martin Hodas − *Institut für Angewandte Physik, Universität Tübingen, 72076 Tübingen, Germany;* orcid.org/0000-0001-6328-1717

Sigrid Bernstorff − *Elettra-Sincrotrone Trieste S.C.p.A., 34149 Trieste, Italy;* orcid.org/0000-0001-6451-5159

Matej Jergel − *Institute of Physics, Slovak Academy of Sciences, 84511 Bratislava, Slovakia; Centre for Advanced Materials Application, 84511 Bratislava, Slovakia;* orcid.org/0000-0002-4482-7881

Eva Majkova − *Institute of Physics, Slovak Academy of Sciences, 84511 Bratislava, Slovakia; Centre for Advanced Materials Application, 84511 Bratislava, Slovakia;* orcid.org/0000-0001-9597-9247

Frank Schreiber − *Institut für Angewandte Physik, Universität Tübingen, 72076 Tübingen, Germany;* orcid.org/0000-0003-3659-6718

Complete contact information is available at: https://pubs.acs.org/10.1021/acs.jpcc.1c01716

Notes

The authors declare no competing financial interest.

■ ACKNOWLEDGMENTS

We acknowledge the financial support of the projects SK-CN-RD-18-0006, APVV-17-0352, APVV-15-0641, APVV-15-0693, APVV-14-0745, 0APVV-18-0480, APVV-19-0465, APVV-19-0365, APVV-14-074, VEGA 2/0041/21,, 2/0149/17, VEGA 2/0129/19, VEGA 2/0081/18, ITMS 26230120002, ITMS 26210120002, DAAD/SAV grant and the funding by the DFG. This work was performed during the implementation of the project Building-up Centre for advanced materials application of the Slovak Academy of Sciences, ITMS project code 313021T081 supported by the Integrated Infrastructure Operational Programme funded by the ERDF. We would also like to thank the Alexander von Humboldt Foundation for financially supporting M. Hodas.

■ REFERENCES

(1) Wang, Q. H.; Kalantar-Zadeh, K.; Kis, A.; Coleman, J. N.; Strano, M. S. Electronics and Optoelectronics of Two-Dimensional Transition Metal Dichalcogenides. *Nat. Nanotechnol.* **2012**, *7* (11), 699−712.

(2) Chhowalla, M.; Shin, H. S.; Eda, G.; Li, L. J.; Loh, K. P.; Zhang, H. The Chemistry of Two-Dimensional Layered Transition Metal Dichalcogenide Nanosheets. *Nat. Chem.* **2013**, *5*, 263−275.

(3) Mak, K. F.; Lee, C.; Hone, J.; Shan, J.; Heinz, T. F. Atomically Thin MoS_2: A New Direct-Gap Semiconductor. *Phys. Rev. Lett.* **2010**, *105* (13), 136805.

(4) Splendiani, A.; Sun, L.; Zhang, Y.; Li, T.; Kim, J.; Chim, C.-Y.; Galli, G.; Wang, F. Emerging Photoluminescence in Monolayer MoS_2. *Nano Lett.* **2010**, *10* (4), 1271−1275.

(5) Cao, T.; Wang, G.; Han, W.; Ye, H.; Zhu, C.; Shi, J.; Niu, Q.; Tan, P.; Wang, E.; Liu, B.; Feng, J. Valley-Selective Circular Dichroism of Monolayer Molybdenum Disulphide. *Nat. Commun.* **2012**, *3*, 887.

(6) Chromik, Š.; Sojková, M.; Vretenár, V.; Rosová, A.; Dobročka, E.; Hulman, M. Influence of GaN/AlGaN/GaN (0001) and Si (100) Substrates on Structural Properties of Extremely Thin MoS_2 Films Grown by Pulsed Laser Deposition. *Appl. Surf. Sci.* **2017**, *395*, 232−236.

(7) Brivio, J.; Alexander, D. T. L.; Kis, A. Ripples and Layers in Ultrathin MoS_2 Membranes. *Nano Lett.* **2011**, *11* (12), 5148−5153.

(8) Jeon, J.; Jang, S. K.; Jeon, S. M.; Yoo, G.; Jang, Y. H.; Park, J.-H.; Lee, S. Layer-Controlled CVD Growth of Large-Area Two-Dimensional MoS_2 Films. *Nanoscale* **2015**, *7* (5), 1688−1695.

(9) Sojková, M.; Vegso, K.; Mrkyvkova, N.; Hagara, J.; Hutár, P.; Rosová, A.; Čaplovičová, M.; Ludacka, U.; Skákalová, V.; Majková, E.; Siffalovic, P.; Hulman, M. Tuning the Orientation of Few-Layer MoS_2 Films Using One-Zone Sulfurization. *RSC Adv.* **2019**, *9* (51), 29645−29651.

(10) Zhang, J.; Yu, H.; Chen, W.; Tian, X.; Liu, D.; Cheng, M.; Xie, G.; Yang, W.; Yang, R.; Bai, X.; Shi, D.; Zhang, G. Scalable Growth of High-Quality Polycrystalline MoS_2 Monolayers on SiO_2 with Tunable Grain Sizes. *ACS Nano* **2014**, *8* (6), 6024−6030.

(11) Wang, X.; Feng, H.; Wu, Y.; Jiao, L. Controlled Synthesis of Highly Crystalline MoS_2 Flakes by Chemical Vapor Deposition. *J. Am. Chem. Soc.* **2013**, *135* (14), 5304−5307.

(12) Lee, Y.-H.; Zhang, X.-Q.; Zhang, W.; Chang, M.-T.; Lin, C.-T.; Chang, K.-D.; Yu, Y.-C.; Wang, J. T.-W.; Chang, C.-S.; Li, L.-J.; Lin, T.-W. Synthesis of Large-Area MoS_2 Atomic Layers with Chemical Vapor Deposition. *Adv. Mater.* **2012**, *24* (17), 2320−2325.

(13) Ji, Q.; Zhang, Y.; Gao, T.; Zhang, Y.; Ma, D.; Liu, M.; Chen, Y.; Qiao, X.; Tan, P.-H.; Kan, M.; Feng, J.; Sun, Q.; Liu, Z. Epitaxial Monolayer MoS_2 on Mica with Novel Photoluminescence. *Nano Lett.* **2013**, *13* (8), 3870−3877.

(14) Choudhary, N.; Chung, H.-S.; Kim, J. H.; Noh, C.; Islam, M. A.; Oh, K. H.; Coffey, K.; Jung, Y.; Jung, Y. Strain-Driven and Layer-Number-Dependent Crossover of Growth Mode in van Der Waals Heterostructures: 2D/2D Layer-By-Layer Horizontal Epitaxy to 2D/3D Vertical Reorientation. *Adv. Mater. Interfaces* **2018**, *5* (14), 1800382.

(15) Radisavljevic, B.; Kis, A. Mobility Engineering and a Metal-Insulator Transition in Monolayer MoS_2. *Nat. Mater.* **2013**, *12* (9), 815−820.

(16) Sanne, A.; Ghosh, R.; Rai, A.; Movva, H. C. P.; Sharma, A.; Rao, R.; Mathew, L.; Banerjee, S. K. Top-Gated Chemical Vapor Deposited MoS_2 Field-Effect Transistors on Si_3N_4 Substrates. *Appl. Phys. Lett.* **2015**, *106* (6), 062101.

(17) Singh, E.; Kim, K. S.; Yeom, G. Y.; Nalwa, H. S. Atomically Thin-Layered Molybdenum Disulfide (MoS_2) for Bulk-Heterojunction Solar Cells. *ACS Appl. Mater. Interfaces* **2017**, *9* (4), 3223−3245.

(18) Liu, C.; Kong, D.; Hsu, P.-C. C.; Yuan, H.; Lee, H.-W. W.; Liu, Y.; Wang, H.; Wang, S.; Yan, K.; Lin, D.; Maraccini, P. A.; Parker, K. M.; Boehm, A. B.; Cui, Y. Rapid Water Disinfection Using Vertically Aligned MoS_2 Nanofilms and Visible Light. *Nat. Nanotechnol.* **2016**, *11* (12), 1098−1104.

(19) Xu, J.; Cao, X. Characterization and Mechanism of MoS_2/CdS Composite Photocatalyst Used for Hydrogen Production from Water Splitting under Visible Light. *Chem. Eng. J.* **2015**, *260*, 642−648.

(20) Kong, D.; Wang, H.; Cha, J. J.; Pasta, M.; Koski, K. J.; Yao, J.; Cui, Y. Synthesis of MoS_2 and $MoSe_2$ Films with Vertically Aligned Layers. *Nano Lett.* **2013**, *13* (3), 1341−1347.

(21) Bodik, M.; Sojkova, M.; Hulman, M.; Tapajna, M.; Truchly, M.; Vegso, K.; Jergel, M.; Majkova, E.; Spankova, M.; Siffalovic, P. Friction Control by Engineering the Crystallographic Orientation of the Lubricating Few-Layer MoS2 Films. *Appl. Surf. Sci.* **2021**, *540*, 148328.

(22) Hagara, J.; Mrkyvkova, N.; Nádaždy, P.; Hodas, M.; Bodík, M.; Jergel, M.; Majková, E.; Tokár, K.; Hutár, P.; Sojková, M.; Chumakov, A.; Konovalov, O.; Pandit, P.; Roth, S.; Hinderhofer, A.; Hulman, M.; Siffalovic, P.; Schreiber, F. Reorientation of π-Conjugated Molecules on Few-Layer MoS_2 Films. *Phys. Chem. Chem. Phys.* **2020**, *22* (5), 3097−3104.

(23) Jäger-Waldau, A.; Lux-Steiner, M. C.; Bucher, E.; Scandella, L.; Schumacher, A.; Prins, R. MoS_2 Thin Films Prepared by Sulphurization. *Appl. Surf. Sci.* **1993**, *65*−*66* (C), 465−472.

(24) Jung, Y.; Shen, J.; Liu, Y.; Woods, J. M.; Sun, Y.; Cha, J. J. Metal Seed Layer Thickness-Induced Transition from Vertical to Horizontal Growth of MoS_2 and WS_2. *Nano Lett.* **2014**, *14* (12), 6842−6849.

(25) Cho, S.-Y.; Kim, S. J.; Lee, Y.; Kim, J.-S.; Jung, W.-B.; Yoo, H.-W.; Kim, J.; Jung, H.-T. Highly Enhanced Gas Adsorption Properties in Vertically Aligned MoS_2 Layers. *ACS Nano* **2015**, *9* (9), 9314−9321.

(26) Shang, S.-L.; Lindwall, G.; Wang, Y.; Redwing, J. M.; Anderson, T.; Liu, Z.-K. Lateral Versus Vertical Growth of Two-Dimensional Layered Transition-Metal Dichalcogenides: Thermodynamic Insight into MoS_2. *Nano Lett.* **2016**, *16* (9), 5742−5750.

(27) Stern, C.; Grinvald, S.; Kirshner, M.; Sinai, O.; Oksman, M.; Alon, H.; Meiron, O. E.; Bar-Sadan, M.; Houben, L.; Naveh, D. Growth Mechanisms and Electronic Properties of Vertically Aligned MoS_2. *Sci. Rep.* **2018**, *8* (1), 16480.

(28) Chen, B.; Yu, Q.; Yang, Q.; Bao, P.; Zhang, W.; Lou, L.; Zhu, W.; Wang, G. Large-Area High Quality MoS_2 Monolayers Grown by Sulfur Vapor Counter Flow Diffusion. *RSC Adv.* **2016**, *6* (55), 50306−50314.

(29) Baker, J. L.; Jimison, L. H.; Mannsfeld, S.; Volkman, S.; Yin, S.; Subramanian, V.; Salleo, A.; Alivisatos, A. P.; Toney, M. F. Quantification of Thin Film Crystallographic Orientation Using X-Ray Diffraction with an Area Detector. *Langmuir* **2010**, *26* (11), 9146−9151.

(30) Brewer, L.; Lamoreaux, R. H. The Mo-S System (Molybdenum-Sulfur). *Bull. Alloy Phase Diagrams* **1980**, *1* (2), 93−95.

(31) Bolhuis, M.; Hernandez-Rueda, J.; van Heijst, S. E.; Tinoco Rivas, M.; Kuipers, L.; Conesa-Boj, S. Vertically-Oriented MoS_2 Nanosheets for Nonlinear Optical Devices. *Nanoscale* **2020**, *12* (19), 10491−10497.

(32) Dutrizac, J. E. The Reaction of Sulphur Vapour with Molybdenum Metal. *Can. Metall. Q.* **1970**, *9* (3), 449−453.

https://doi.org/10.1021/acs.jpcc.1c01716
J. Phys. Chem. C 2021, 125, 9461−9468

(33) Avrami, M. Kinetics of Phase Change. I: General Theory. *J. Chem. Phys.* **1939**, *7*, 1103−1112.
(34) Avrami, M. Kinetics of Phase Change. II Transformation-Time Relations for Random Distribution of Nuclei. *J. Chem. Phys.* **1940**, *8*, 212−224.
(35) Avrami, M. Granulation, Phase Change, and Microstructure Kinetics of Phase Change. III. *J. Chem. Phys.* **1941**, *9*, 177−184.
(36) Dietz, W. Sphärolithwachstum in Polymeren. *Colloid Polym. Sci.* **1981**, *259*, 413−429.
(37) Shan, H.; Lickfield, G. C. Crystallization Kinetics Study of Polyethylene. *Int. J. Polym. Anal. Charact.* **2007**, *12* (4), 327−338.
(38) Albano, C.; Papa, J.; Ichazo, M.; González, J.; Ustariz, C. Application of Different Macrokinetic Models to the Isothermal Crystallization of PP/Talc Blends. *Compos. Struct.* **2003**, *62* (3−4), 291−302.
(39) Fueki, K.; Ishibashi, H.; Mukaibo, T. Kinetic Studies on Sulfidization of Metals. *J. Electrochem. Soc. Jpn.* **1962**, *30* (1), E23−E29.
(40) Verble, J. L.; Wietling, T. J.; Reed, P. R. Rigid-Layer Lattice Vibrations and van Der Waals Bonding in Hexagonal MoS_2. *Solid State Commun.* **1972**, *11* (8), 941−944.

https://doi.org/10.1021/acs.jpcc.1c01716
J. Phys. Chem. C 2021, 125, 9461−9468